



HAL
open science

Very low-grade metamorphism in the para-autochthonous sedimentary cover of the Pelvoux massif (Western Alps, France)

Sébastien Potel, Ghislain Trullenque

► **To cite this version:**

Sébastien Potel, Ghislain Trullenque. Very low-grade metamorphism in the para-autochthonous sedimentary cover of the Pelvoux massif (Western Alps, France). *Swiss Journal of Geosciences*, 2012, 105 (2), pp.235-247. 10.1007/s00015-012-0102-8. hal-03683486

HAL Id: hal-03683486

<https://hal.science/hal-03683486v1>

Submitted on 31 May 2022

HAL is a multi-disciplinary open access archive for the deposit and dissemination of scientific research documents, whether they are published or not. The documents may come from teaching and research institutions in France or abroad, or from public or private research centers.

L'archive ouverte pluridisciplinaire **HAL**, est destinée au dépôt et à la diffusion de documents scientifiques de niveau recherche, publiés ou non, émanant des établissements d'enseignement et de recherche français ou étrangers, des laboratoires publics ou privés.

1 **Very low-grade metamorphism in the para-autochthonous sedimentary cover of the**
2 **Pelvoux massif (Western Alps, France).**

3

4 Sébastien Potel^{(1), (2)} & Ghislain Trullenque^{(3), (4)}

5

6 ⁽¹⁾ Present address: Institut Polytechnique LaSalle Beauvais - Equipe B2R, 19 rue Pierre
7 Wagnet, BP 30313 – F-60026 BEAUVAIS Cedex.

8 ⁽²⁾ Insitut für Geowissenschaften und Lithosphärenforschung, Universität Giessen, Germany.

9

10 ⁽³⁾ Present address: Institut für Geowissenschaften, Geologie, Universität Freiburg, Albertstr.
11 23b, Freiburg, Germany.

12 ⁽⁴⁾ Institute of Geology and Paleontology, University of Basel.

13

14

15 Keywords: Illite crystallinity, very low-grade metamorphism, Western Alps, external
16 crystalline massif.

17

18 **Abstract**

19 The metamorphic grade from the para-autochthonous cover of the Pelvoux Massif (PM,
20 western Alps, France) was investigated in Priabonian metamarls, through mineral
21 assemblages, simultaneous measurements of illite and chlorite “crystallinity”, K-white mica *b*
22 cell dimension and K-white mica polytypes content. Kübler (KI) and Árkai (ÁI) indexes
23 display values characteristic for uppermost diagenetic to low anchizonal conditions. These
24 results are supported by the incomplete transformation of K-white mica polytypes from 1M_d
25 to 2M₁ and are in line with the not annealed status of zircon fission tracks in the southeast
26 zone of the Pelvoux Massif (Seward et al. 1999). Our findings differ from previous results,
27 which suggested epizonal conditions at several places in the northern part of our field area,
28 but are coherent with the temperature estimation suggested by the mineral assemblage
29 described in the literature. These results are further supported by temperature values deduced
30 from fluid inclusion investigations. A small decrease of KI and ÁI values is observed within
31 the basal decollement level of the Priabonian cover, when going from the least deformed
32 zones to the most deformed ones. K-white mica *b* cell dimensions in micas of the area are in
33 the range 9.000-9.040 Å, which corresponds to an inferred geothermal gradient of 25-
34 35°C/Km, similar to the values found further north in the Dauphinois domain (Ceriani et al.
35 2003). Based on Ferreiro Máhlmann (2001), this can supposed a long stady state heat flow
36 corresponding to a long term metamorphic event like in the eastern Alps.

37

38 **1 Introduction**

39 In the western Alps, the illite “crystallinity” method has been used in order to differentiate the
40 anchizone from diagenesis and epizone domains according to Kübler (1968). The general
41 trend of the metamorphic grade, increasing from W to E, from diagenesis to epizone, is

42 perturbed by tectonic duplexes and the influence of crystalline basement (Desmons et al.
43 1999).

44

45 In the northern part of the Pelvoux massif, Ceriani et al. (2003) studied the low-grade
46 metamorphism in the region of the Frontal Penninic units (FPU) of the Western Alps between
47 the Arc and Isère Valleys (Fig. 1a-b). The results of the study allowed relating the
48 metamorphism to the different stages of deformation.

49

50 Previous metamorphic studies described south of the Pelvoux massif a laumontite-prehnite-
51 pumpellyite subfacies (zeolite facies) in the “grès de Champsaur” formation, with rock-
52 forming laumontite (Aprahmian 1988) and pumpellyite-prehnite in veins (Waibel 1990). On
53 the metamorphic map of the Alps (Frey et al. 1999) and the map of metamorphic structure of
54 the Alps (Oberhänsli et al. 2004) the sub-greenschist facies (epizone) is found in the tiny
55 basement of Fournel and Dormillouse valleys (cf. Fig 1b).

56

57 The aim of this contribution is to present the results of a study on metamorphic grade in the
58 southern footwall of the Penninic Basal Contact (PBC, Ceriani et al. 2001), within the
59 Dauphinois cover of the southeastern rim of the Pelvoux Massif, and to compare the results
60 with those from Ceriani et al. (2003). The metamorphic grade was investigated in the
61 globigerina metamarls level and in the Mesozoic cover by mineral assemblages, simultaneous
62 measurements of illite and chlorite “crystallinity” using the KI- and AI- methods, K-white
63 mica *b* cell dimension and K-white mica polytypes content. Within the Rocher de l’Yret shear
64 zone (RYSZ, Fig. 1), results are completed by a fluid inclusion study. Quartz precipitates found
65 along the strike slip fault planes dissecting the uppermost basement units from the RYSZ
66 were analysed. All the methods were used for a better P-T estimate to get a higher precision

67 on the metamorphic evolution in this region and to conclude better with some geodynamic
68 implications. The results of this metamorphic study are compared to those from Ceriani et al.
69 (2003) north of the Pelvoux massif, to the FT data available in the region (Seward et al. 1999;
70 Fügenschuh and Schmid 2003) and previous studies describing mineral assemblage in the
71 “grès de Champsaur” (Aprahamian 1988; Waibel 1990).

72

73 **2 Regional Geology**

74 The Dauphinois domain is part of the European margin and composed of Variscan basement
75 carrying a thick Permian to Tertiary sedimentary cover. During Mesozoic rifting, the eastern
76 margin of the European plate was substantially thinned. Formation of major tilted crustal
77 blocks allowed for the deposition of thick Mesozoic sedimentary series in asymmetric half
78 grabens intensively described in literature (Tricart et al. 1988; Davies 1982; Gillcrist et al.
79 1987; Butler 1989; Coward et al. 1991; Huyghe and Mugnier 1995; Lazarre et al. 1996; Sue
80 et al. 1997).

81 Mesozoic strata are discordantly overlain by a conglomerate formation (Gupta 1997),
82 followed by the classical “Priabonian trilogy” (Ravenne 1987; Apps et al. 2004), which
83 comprises, from base to top: (1) shallow water nummulitic limestone of variable thickness (0
84 - 50 m), (2) hemipelagic globigerina marls (0 - 50 m), (3) the “grès de Champsaur” formation,
85 a regular alternance of turbiditic sandstones and shales (Perriaux and Uselle 1968; Waibel
86 1990), whose thickness varies from 700 to 1200 meters. In some areas immediately south of
87 the Pelvoux Massif, the silici-clastic deposits contain up to 50% of volcanic detritus
88 (Debrand-Passard et al. 1984; Bürgisser 1998).

89 Locally, three Alpine deformation phases (D_1 , D_2 and D_3) can be recognized (Trullenque,
90 2005). D_1 , first phase of deformation that affected the Dauphinois units corresponds to the
91 third phase of deformation described by Ceriani et al. 2001, i.e Oligocene to lower Miocene

92 out of sequence thrusting along the Roselend thrust (RT). It is the major deformation phase
93 encountered in the investigated area since it is related to the thrusting along the RT (Ceriani et
94 al. 2001). D₁ deformation structures constantly show WNW-directed kinematic indicators
95 measured directly along tectonic contacts, i.e. consistent with activity along the RT.

96 The second D₂ deformation phase recorded within the investigated area results in SW-
97 directed movements that overprint the top-WNW D₁ deformation features and which are
98 missing N of the Pelvoux massif. Trullenque (2005) proposed that the D₂ top-SW
99 deformation phase is linked to the formation of the Apeninnes chain, as a consequence of the
100 opening of the Thyrenian basin during Langhian times.

101 D₃ structures, normal faults related to the Durance fault system (High Durance Faulted Zone,
102 Tricart 2004) are the latest deformation features found in the investigated area. These normal
103 faults are notably responsible for a strong geothermal gradient and seismicity recorded along
104 the Durance valley. The timing of the onset of normal faulting, also recorded north of
105 Pelvoux, remains a matter of debate in literature (see Fügenschuh et al. 1999; Fügenschuh and
106 Schmid 2003; Tricart et al. 2001). However, in this region, fission track data on zircon
107 (Seward et al. 1999) reveal that maximum temperatures were well below greenschist facies
108 conditions. Seward et al. (1999) interpreted the heating event as being due to the
109 emplacement of internal thrust sheets, which thin out westwards.

110

111 **3 Material and methods**

112 In marine pelites and carbonates, no diagnostic minerals and mineral assemblages form at
113 conditions of very low-grade field. In these rocks, the transitions from non-metamorphic to
114 very low-grade and from very low-grade to low-grade metamorphic domains take place
115 through the diagenetic zone, the anchizone and the epizone, each zone being characterized by
116 specific values of the illite Kübler Index (Árkai et al. 2003). The illite "crystallinity" (IC or

117 Kübler index (KI; Kübler 1964) is defined as the full width at half maximum of the first illite
118 basal reflection in XRD patterns (Frey 1987; Guggenheim et al. 2002). Guggenheim et al.
119 (2002) recommended that the use of a “crystallinity index” should be avoided, although it
120 may be placed within quotation marks when referring in a limited way to previously
121 referenced work. They also recommended to refer to an index by relating it to the author
122 describing the procedures necessary to define the value, regardless of what the index may
123 actually be describing. Therefore, we will refer for K-white mica to the illite “crystallinity”
124 for raw data and to Kübler index after calibration against Kübler’s scale.

125 Illite “crystallinity” is considered to be a function of crystallite thickness, the number of
126 lattice defects (Merriman et al. 1990). Temperature is thought to be the main factor
127 controlling the illite “crystallinity”, but other parameters like lithology, time, tectonic stress
128 and fluid/rock ratio may probably have important effect (see Frey 1987). Árkai (1991) and
129 Árkai et al. (1995) proposed a similar index the chlorite “crystallinity” (ChC) or Árkai index
130 (ÁI) to monitor the reaction’s progress.

131 Twenty-four metamarls samples were collected within the Priabonian and Mesozoic cover
132 formations of the Dauphinois. Sampling was restricted to these formations in order to
133 minimize the petrological effect on the IC. The outcrops density also limited the sampling
134 area, around the Dormillouse and Fournel valleys outcrops are poor. Moreover, westward the
135 Selle Fault cut out the Priabonian formation. The nature, age and tectonic setting of this fault
136 are poorly constrained leading to uncertainties on its effects on the metamorphic pattern.
137 Therefore, samples were taken in the Dormillouse, Fournel, Beassac and Chambran valleys
138 and in the Yret zone (Figs. 1 and 2).

139 In the different samples, the main schistosity is related to the D₁ phase (Trullenque 2005),
140 the D₂ phase only affects the area south of an E-W line of Beassac valley. The clay fraction
141 analysed is generally related to D₁.

142 Samples with detrital mica visible in hand specimen and/or weathered specimens were
143 avoided as far as possible to eliminate detrital contamination. Mineral abbreviations used are
144 from Kretz (1983).

145

146 1. X-ray diffraction

147 Clay mineral separation was conducted using techniques described by Potel et al. (2006).
148 Carbonate removal was done using a 5% acetic acid ($C_2H_4O_2$) and washed after with
149 deionised water. To minimize the effect of possible detrital clay minerals, we avoided long
150 grinding processes (< 15 sec) and repeated the settling procedure for the $\leq 2\mu m$ fraction 5
151 times. Illite and chlorite crystallinity was measured at the University of Giessen on air-dried
152 preparates, using a D501 Bruker-AXS (Siemens) diffractometer, $CuK\alpha$ radiation at 40 kV &
153 30 mA and divergence slits of 0.5° with a secondary graphite monochromator. Two slices of
154 each sample were prepared and each measured two times as air-dried and one time glycolated.
155 The range of measurement, the time counting and the step size were as follow: for whole-rock
156 paragenesis between 2 and $70 \Delta^2\Theta$ with 1 sec and 0.02° step, for air-dried preparate between
157 2 and $70 \Delta^2\Theta$ with 2 sec and 0.01° step.

158 IC was calculated using the software DIFFRACPlus (evaluation/release 2001 by ©Bruker
159 AXS) and MacDiff 4.25 (written by R. Petschick, 17 May 2001). IC measured in Giessen
160 ($IC_{Giessen}$) values were transformed into KI values using a correlation with the SW standards
161 (CIS standards) of Warr and Rice (1994) ($KI_{CIS} = 1.2702 * IC_{Giessen} - 0.0314$) (Table 1). The
162 Kübler index was used to define the limits of anchizone, and the transition values were
163 chosen as follows: $KI = 0.25 \Delta^2\Theta$ for the epizone to high anchizone boundary, $KI = 0.30$
164 $\Delta^2\Theta$ for the high to low anchizone boundary and $KI = 0.42 \Delta^2\Theta$ for the low anchizone to
165 diagenetic zone. However, the use of the CIS standards is not universally accepted as giving

166 Kübler-equivalent zone limits. Kisch et al. (2004) show that the CIS standard values are much
167 broader than those obtained by all other laboratories and that the high- and low-grade
168 boundaries of the anchizone of the raw values of Warr and Rice (1994) are much broader than
169 the Kübler-equivalent. This discrepancy is likely to reflect errors in the conversion of the IC
170 values into Kübler equivalent (Kisch et al. 2004; Ferreiro Mählmann and Frey this volume;
171 Ferreiro Mählmann et al. this volume). Therefore, following the recommendations done by
172 Kisch et al. (2004), we published in the Table 1 the IC_{Giessen} and ChC to allow comparison
173 with other laboratories. The same experimental conditions were also used to determine
174 chlorite “crystallinity” on the (002) peak of the second (7 Å) basal reflections of chlorite
175 (Table 1). The ChC measurements were calibrated with those of Warr and Rice (1994) and
176 expressed as the Árkai index (ÁI) (Guggenheim et al. 2002): $\mathbf{\acute{A}I = 0.8775 * ChC + 0.0239}$.
177 The anchizone boundaries for the Árkai index were defined by correlation with the Kübler
178 index and are given as 0.24 $\Delta^{\circ}2\Theta$ for the epizone to anchizone boundary and 0.30 $\Delta^{\circ}2\Theta$ for
179 the anchizone to diagenetic zone.

180 Randomly oriented samples for K-white mica *b* cell dimension and polytype determination
181 of K-white mica were prepared using wood glue on quartz sample holder. The K-white mica
182 *b* cell dimension is based on the $d_{060,331}$ spacing and on the increasing celadonite substitution
183 that occurs with pressure increase in white mica (Ernst 1963; Guidotti et al. 1989). Guidotti et
184 al. (1989) presented linear regression equations that quantify the changes in the K-white mica
185 *b* cell dimensions of muscovite 2M₁ that result from cation substitutions on the interlayer and
186 octahedral sites. The K-white mica *b* cell dimension value was determined by measurement of
187 the (060) peak of the potassic white mica, if present (Sassi and Scolari 1974), by using the
188 cell-refinement program WIN-METRIC V.3.0.7 (©Bruker AXS).

189 Illite-muscovite polytype determination was done using a curve of 2M₁/(2M₁+1M) peaks
190 ratio calibrated using different mixture of illite polytype following the technique described by

191 Dalla Torre et al. (1994). Merriman and Peacor (1999) recognized that the wealth of data on
192 variations in white mica polytypism as a function of temperature is generally consistent with
193 predictable trends. However, they recommended that polytype sequences should not be used
194 other than as indicators of reaction progress.

195

196 2. *Microthermometry*

197 Quartz-calcite veins were sampled along the Rocher de l'Yret shear zone (RYSZ) (Figs. 1 &
198 2), in order to substantiate P-T estimation and to reconstruct the fluid evolution history during
199 metamorphism (Frey et al. 1980). Microthermometry investigations were done at the
200 University of Giessen on double polished thin sections and performed using a Linkam THM
201 600/S/Geo heating-freezing stage coupled to a TMS 94 temperature controller with an error of
202 $\pm 1^\circ\text{C}$. The stage is mounted on an Olympus microscope with a 100X Objective. The heating
203 and cooling stage was calibrated using synthetic fluid inclusion calibration standard: CO₂ and
204 H₂O from ©Bubbles Incorporation.

205 Two-phase (consisting of vapour and liquid at room temperature) fluid inclusions were
206 identified. No dissolved volatile phase was observed, either by melting of CO₂ at or below its
207 triple point of -56.6°C , nor by formation or dissolution of clathrate or liquid-vapor
208 equilibrium of a volatile component such as higher hydrocarbons (HHC), CH₄, CO₂, N₂ or
209 H₂S. Thus, microthermometry was restricted to measuring the melting temperature of ice
210 ($T_{m_{\text{ice}}}$) and the bulk homogenization temperature of the fluid inclusions (T_{h_i}). As none of the
211 investigated fluid inclusions contained any observable gas component, salinity was derived
212 from the ice melting temperature in NaCl-equivalence after Hall et al. (1988). Density for
213 fluid inclusions with homogenisation temperatures less than 200°C are from the equations of
214 state given by Brown and Lamb (1989) and for temperatures greater than 200°C are from

215 Zhang and Frantz (1987). The isochores were calculated from the equation of state given by
216 Zhang and Frantz (1987).

217

218 3. Raman microspectrometry

219 Gas, liquid and solid phases were investigated at the University of Frankfurt am Main
220 using a Raman microprobe Leica/Renishaw and the software Renishaw WiRE™ 2.0 and
221 GRAMS. An Argon laser (green laser: $\lambda = 514.5 \text{ nm}^{-1}$) was used as excitation laser radiation.
222 The Raman microspectrometry was used to identify the presence of CH₄, CO₂, HHC (C₂H₆ or
223 C₃H₈) and N₂ in fluid inclusions. The relevant peak is positioned at 2917cm⁻¹ for CH₄, 1285
224 and 1388 cm⁻¹ for CO₂, 2890 and 2954cm⁻¹ for C₂H₆ or C₃H₈ respectively and 2331cm⁻¹ for
225 N₂ (Burke 2001). The small size of most fluid inclusions (< 10µm) and the large vertical
226 dimension of the laser beam focus (4µm in diameter) cause the presence of Raman lines of
227 the enclosing quartz (1160cm⁻¹) in the spectra of fluids. This line does not interfere at all with
228 the CH₄, CO₂ and N₂ lines.

229

230 4 Results

231 1. Mineralogy

232 The mineralogy of the studied samples is given in Table 1.

233 In the Priabonian and Mesozoic meta-marls, the mineral assemblages consist of quartz +
234 K-white micas + chlorite and calcite with minor amounts of albite. Gypsum is detected in
235 some samples from the Fournel and Dormillouse valleys (Do2, Fo3a and Fo3c). In the
236 fraction <2 µm, illite-muscovite predominates, chlorite and quartz are significant, and
237 feldspar, if detected, is only present in small quantities.

238

239 2. *Characteristics of the phyllosilicates*

240 Figure 2 shows the distribution of the KI data, the values of which are listed in Table 1.

241 The values in the Dormillouse valley vary between uppermost diagenetic conditions
242 (0.43 $\Delta^{\circ}2\Theta$) in the south and low anchizonal values (0.36 $\Delta^{\circ}2\Theta$) in the north. In the Fournel,
243 Beassac and Chambran Valleys, the KI data indicate low anchizonal conditions (0.35 to
244 0.41 $\Delta^{\circ}2\Theta$). In the Yret Zone, illite crystallinity values correspond to the
245 diagenesis/anchizone boundary (0.37 to 0.43 $\Delta^{\circ}2\Theta$) (Fig. 2). No trend can be observed
246 between KI and elevation of the sample. However, a trend can be observed in each valley or
247 zone, with an increase from south to north of KI values. This is similar to that Aprahamian
248 (1988) described.

249 Figure 2 presents the distribution of $\acute{A}I$ values in the studied area. The pattern of very low-
250 grade metamorphism shown by $\acute{A}I$ agrees well with the pattern of the KI (Fig. 2). A positive
251 linear correlation ($R^2 = 0.64$) is found between KI and $\acute{A}I$ values (Fig. 3a). This gives
252 confidence on the fact that illite and chlorite “crystallinities” actually refer to the same P-T
253 conditions and thus the same experienced T-t history.

254 The percentage of $2M_1$ illite-muscovite polytype relative to the KI in the studied area
255 shows a positive trend with increasing metamorphic grade (Fig. 3b).

256 Sassi and Scolari (1974) determined a semi quantitative relationship between the K-white
257 mica b cell dimension and the metamorphic pressure gradient under greenschist facies
258 condition. They plotted the K-white mica b -values as cumulative frequency curves in order to
259 compare them with other metamorphic belts. Guidotti and Sassi (1986) collated published K-
260 white mica b cell dimension data for greenschist and blueschist facies rocks. They presented a
261 qualitative plot of b cell dimension as a family of curves in P-T space. The values presented
262 by Guidotti and Sassi (1986) do not extend to the sub-greenschist facies. However, the
263 considerable amount of K-white mica b cell dimension data from very low-grade metapelites

264 accumulated in different metamorphic belt corroborate the groupings found by Guidotti and
265 Sassi (1986), as shown by Merriman and Peacor (1999). K-white mica *b* cell dimensions were
266 calculated for 21 samples from the anchizone (three samples were not integrated due to
267 interferences and poor intensity signal), all fall in the same range with a minimum 8.998 and a
268 maximum 9.028 Å values (Table 1). Specimens from the Mesozoic cover have lower values
269 (at around 9.000 Å), while Priabonian are centred around 9.020 Å. However, both value
270 groups are in the intermediate pressure facies (between 9.000 and 9.040 Å) as shown in
271 Figure 4 (the curve obtained is similar to the reference curve from Ryoike), suggesting an
272 inferred geothermal gradient of 25-35°C/km (Guidotti and Sassi 1986).

273 3. *Vein mineralogy, textural relationships and microthermometry*

274 Samples were collected within the RYSZ, previously described by Butler (1992), and
275 consisting in an imbricate of basement slices and para-autochthonous sedimentary cover. This
276 shear zone, lying directly below the frontal penninic nappe stack, has been considered as the
277 map trace of the RT in this area (Trullenque 2005). All kinematic indicators measured in the
278 field or deduced from microfabric analysis of calcite ultramytonites (Trullenque 2006),
279 consistently show a WNW directed sense of transport, consistent with activity along the RT.
280 No evidence of D₂ structures are found in this area.

281 Samples have been collected along strike slip fault planes dissecting basement slices and
282 indicating a clear WNW directed sense of transport. These faults are clearly related to the first
283 deformation phase D₁. The chronology of the different fluid inclusion populations (Table 2) is
284 a relative one with respect to their host mineral and their overgrowth (Mullis 1976).

285 Veins are mainly composed of small quartz crystals associated sometimes with calcite
286 crystals. Only two-phase fluid inclusions (consisting of vapour and liquid at room
287 temperature) were identified with the microscope. Fibre quartz is observed in the sample F72.
288 In F92, two fluid inclusion assemblages are identified. The first one is a two-phase type in the

289 host quartz and probably of primary type, i.e. trapped during mineral growth. The second one
290 is overprinting the first assemblage and probably of pseudo-secondary type. The true
291 temperature of entrapment of the fluid inclusions, i.e. mineral growth, was constrained by
292 intersecting the isochores of primary two-type phase fluid inclusions with the inferred
293 geothermal gradient deduced from the K-white b cell dimension (Fig. 5). Isochores were
294 calculated for the lower and upper homogenization temperature (T_{hi}) with an average salinity
295 of 5.6 and 13.8wt.% NaCl equivalent for samples F72 and F92, respectively.

296

297 **5 Discussion**

298 The structural metamorphic map of the Alps (Oberhänsli et al. 2004) indicates lower sub-
299 greenschist facies E of the RT and N of the Pelvoux massif. North of the Pelvoux massif,
300 Ceriani et al. (2003) described an E-W metamorphic gradient on the E side of the RT. In the
301 Briançonnais, they reported an increase from anchizonal to epizonal conditions from E to W.
302 In the same area, the Dauphinois domain (in the footwall of the RT) shows epizonal
303 metamorphic conditions. The Dauphinois domain in this area is only affected by one
304 deformation phase, corresponding to the third deformation phase in the FPU (Ceriani 2001;
305 Ceriani et al. 2001) and equivalent to D_1 in our studied area (Trullenque 2005). The K-white *b*
306 cell dimensions obtained by Ceriani et al. (2003) in the Dauphinois Domain are ranging
307 between 9.000 and 9.030Å similar to those obtained in our study, indicating similar
308 geothermal metamorphic gradient between the two areas.

309 Frey (1987) and Essene and Peacor (1995) showed that KI cannot be used as a precise
310 geothermometer and only provide an approximate temperature range. In spite of this, attempts
311 have been made to relate KI values to absolute temperatures. This was done in different low-
312 grade metamorphic units by comparing the KI data with other geothermometers (Ferreiro
313 Mählmann 1994, 1996; Merriman and Frey 1999; Mullis et al. 2002; Potel et al. 2006). Mullis

314 et al. (2002) have suggested a diagenesis – anchizone boundary in the Alps on the basis of a
315 comparison of IC versus FI data. This allows to better define the range of temperature that the
316 SE of the Pelvoux massif was subjected during tectonic evolution.

317 The KI values indicate that the Dauphinois domain in the SE of the Pelvoux massif
318 underwent up to low anchizonal metamorphic conditions (Table 1; Fig. 2). According to
319 Mullis et al. (2002), the boundary is linked to a temperature of around 230-240°C (similar to
320 the compilation results from Ferreiro Mählmann (1994)). This can be compared to the
321 temperature estimates obtained west of our studied area in the “grès de Champsaur” (W of
322 Prapic). Waibel (1990) described quartz-prehnite±calcite veins in the “grès de Champsaur”.
323 The country rock is dark green in colour, enriched in pumpellyite of variable composition,
324 and to a lesser extent prehnite, at the expense of laumontite. Aprahamian (1988) described
325 also mottled sandstone (faciès moucheté), the pale-coloured mottles being enriched in
326 laumontite as cement and as partial replacement product of albitized clastic plagioclase and
327 the darker areas being relatively enriched in chlorite cement. According to Frey et al. (1991)
328 and Potel et al. (2002), the coexistence of zeolites (laumontite in this case) and prehnite-
329 pumpellyite is restricted to a rather small P-T area below 240°C and therefore in the range
330 obtained by using the correlation from Mullis et al. (2002).

331 Zircon FT data were gained from the turbiditic “grès de Champsaur” and the underlying
332 Pelvoux crystalline basement (Seward et al. 1999). These data provide important information
333 on the peak temperatures reached during Alpine metamorphism. For the zircon FT system,
334 several estimates on the temperature range of the partial annealing zone exist (e.g. Yamada et
335 al. 1995, Tagami et al. 1998, Yamada et al. 2007). Tagami et al. (1996) suggested a
336 temperature range between 200 and 320°C to be appropriate, which covers the temperature
337 range relevant to the metamorphic zonation based on illite “crystallinity” (e.g. Mullis et al.
338 2002). The combination of both methods therefore provides additional constraints on the

339 maximum temperature reached to the SE of the Pelvoux massif. In the Glarus Alps, the
340 comparison between fluid inclusion data and zircon FT data suggests that zircon FT annealing
341 in the Taveyanne sandstone (a lateral equivalent of the “grès de Champsaur”) only become
342 detectable above 250 °C (Rahn 2001). The measured K-white mica *b* cell dimension values
343 inferred intermediate geothermal gradient with 25-35°C/km (Merriman and Peacor 1999).
344 This gradient seems to be a very conservative approach, however this result is similar to that
345 we can found in the Dauphinois domain north of the Pelvoux Massif (Ceriani et al. 2003).
346 Combining this information with the fluid inclusion data obtained in the Yret zone, a trapping
347 temperature for the fluid inclusions of $220 \pm 10^\circ\text{C}$ can be obtained (Figs. 5a & 5b).
348 Consequently, the comparison of KI, FT and fluid inclusion leads to the conclusion that the
349 SE of the Pelvoux massif was subjected to temperatures higher than 200°C, but lower than
350 250°C. This is higher than the estimation of temperature by Seward et al. (1999) who
351 estimated that the burial temperature of the “grès de Champsaur” was not higher than 200°C.
352 This implies metamorphic burial between 7 and 9 km. Neither our KI nor the FT data (Seward
353 et al. 1999) reveal the presence of a metamorphic gradient from E to W in the SE of the
354 Pelvoux massif as described by Aprahamian (1974). The absence of epizonal KI values in the
355 Vallouise valley (Aprahamian 1974, 1988), moves the anchizone-epizone boundary to the N
356 of the Pelvoux massif, where epizonal metamorphic conditions are observed (Ceriani et al.
357 2003). As mentioned by Ferreiro Málhmann and Frey (2012), one of the reasons of the lack of
358 epizonal values, is that the KI values obtained by CIS calibration led to a broadening of the
359 anchizone area.

360 The available metamorphic data from the south of the Pelvoux massif combined with the
361 available deformation data allow us to deduce some conclusions concerning the tectono-
362 metamorphic evolution in this area. A first important result provided by the KI, fluid
363 inclusion and FT data is the fact that the Dauphinois domain exhibits lower metamorphic

364 conditions compared to the Penninic domain. According to the metamorphic map of the Alps,
365 the Penninic domain west of the RT is metamorphosed under lower greenschist facies
366 (Oberhänsli et al. 2004). Field evidences SE of the Pelvoux massif (this paper, Trullenque
367 2005), indicate that D_1 corresponds to the first penetrative schistosity, marked by very fine-
368 grained K-white mica, chlorite, quartz and albite. The metamorphic gradient observed and the
369 formation of the fluid inclusions studied are related to this deformation phase and the burial
370 heating (with a maximum of 9 km burial) was generated by the overthrust Penninic domain
371 along the RT onto the Dauphinois domain. As mentioned above, the K-white mica *b* cell
372 dimension values in our studied area SE of the Pelvoux massif, are similar to those obtained
373 in the north by Ceriani et al. (2003). Therefore, the metamorphic gradient observed in the
374 Penninic domain must be established before D_1 , as observed by Ceriani et al. (2003) further to
375 the N (the D_1 observed SE of the Pelvoux massif correspond to the D_3 , see above). So, we
376 have no trace of an older metamorphic event.

377 North of the Pelvoux massif, the metamorphic grade is higher with epizonal conditions and
378 may be explained by thicker Penninic units on top of the Dauphinois domain leading to higher
379 degree of burial and therefore show a regional metamorphic gradient increasing from S to N.
380 This is corroborated by the same pressure gradient observed north and south of the Pelvoux
381 massif in the Dauphinois domain (same range of K-white mica *b* cell dimension).

382 Ferreiro Mählmann (2001) in the eastern Alps showed that in rocks submitted to a long
383 metamorphic event (20 Ma) and a steady state heat flow, the smectite content in the anchizone
384 is between 0 and 5% (90% of the samples without smectite), and that under stable thermal
385 conditions (equilibrium), KI can be used as a thermometer. In this region, Henrichs (1993)
386 reported K-white mica *b* cell dimension values between 9.000 and 9.022 Å and the
387 compilation of the Ferreiro Mählmann et al. (2012) shows a normal to low geothermal
388 gradient (30°C/km). Comparison of our results with KI and K-white mica *b* cell dimension

389 values will suggest that the Dauphinois Domain has been submitted to a relative long heating
390 time like in the eastern Alps.

391

392 **Conclusion**

393 The tectono-metamorphic history of the Dauphinois domain in the SE of the Pelvoux is
394 similar that described by Ceriani et al. (2003) in the north. Peak metamorphic conditions in
395 the Dauphinois domain are reached during the overthrusting of the Penninic units during D₁
396 top-WNW directed thrusting along the RT. The metamorphism is characterized by
397 temperatures below 250°C and higher than 200°C and a metamorphic gradient between 25
398 and 35°C, and a long time event. This range of temperature is compatible with the FT data
399 published by Seward et al. (1999) indicating that the burial temperature in the region was
400 lower than 250°C. Based on our KI values and the mineral paragenese observed in the W of
401 the “grès de Champsaur”, no E-W metamorphic zonation as described by Aprahamian (1974,
402 1988) is observed. But, in the studied area, the grade of metamorphism in the Dauphinois
403 Domain is lower than in the northern of the Pelvoux massif (Ceriani et al. 2003) confirming
404 the N-S metamorphic zonation described by Aprahamian (1974, 1988). This is also outlined
405 by the zircon FT ages indicating an increase in age primarily from the north to the south
406 (Fügenschuh and Schmid, 2003) and supports their hypothesis that the more southerly located
407 areas were less deeply buried and hence less exhumed. Like proposed by Ceriani et al. (2001)
408 and Fügenschuh and Schmid (2003), the overthrust along the RT of the Penninic units may
409 caused burial and metamorphism in the external Dauphinois units.

410

411 **Acknowledgements**

412 This manuscript benefited greatly from constructive and helpful reviews and comments from
413 M. Rahn and R. Ferreiro Mählmann.

414

415

416 **References**

417

418 Apps, G.M., Peel, F. & Elliott, T. (2004). The structural setting and palaeogeographical
419 evolution of the Gres d'Annot Basin. Deep-water sedimentation in the Alpine Basin of
420 SE France; new perspectives on the Gres d'Annot and related systems. *Geological*
421 *Society Special Publication*, 221, 65-96.

422 Aprahamian, J. (1974). La cristallinité de l'illite et les minéraux argileux en bordure des
423 massifs cristallins externes de Belledonne et du Pelvoux. *Géologie Alpine*, 50, 5-15.

424 Aprahamian, J. (1988). Cartographie du métamorphisme faible à très faible dans les Alpes
425 françaises externes par l'utilisation de la cristallinité de l'illite. *Geodinamica Acta*, 2, 25-
426 32.

427 Árkai P. (1991). Chlorite crystallinity: an empirical approach and correlation with illite
428 crystallinity, coal rank and mineral facies as exemplified by Palaeozoic and Mesozoic
429 rocks of northeast Hungary. *Journal of Metamorphic Geology*, 9, 723-734.

430 Árkai, P., Sassi, F.P. & Sassi, R. (1995). Simultaneous measurements of chlorite and illite
431 crystallinity: a more reliable tool for monitoring low- to very low grade metamorphism in
432 metapelites. A case study from the Southern Alps (NE Italy). *European Journal*
433 *Mineralogy*, 7, 1115-1128.

434 Árkai, P., Faryad, S.W., Vidal, O. & Balogh, K. (2003). Very low-grade metamorphism of
435 sedimentary rocks of the Meliata unit, Western Carpathians, Slovakia: Implications of
436 phyllosilicate characteristics. *International Journal of Earth Sciences*, 92, 68-85.

437 Brown, P.E., & Lamb, W.M. (1989). P-V-T properties of fluids in the system
438 $H_2O \pm CO_2 \pm NaCl$: New graphical presentations and implications for fluid inclusion
439 studies. *Geochimica Cosmochimica Acta*, 53, 1209-1221.

440 Burke, E.A.J. (2001). Raman microspectrometry of fluid inclusions. *Lithos*, 55, 139-158.

441 Bürgisser, J. (1998). Deformation in foreland basins of the Western Alps (Pelvoux massif, SE
442 France); significance for the development of the Alpine arc. ETH, Zürich, 151 pp.

443 Butler, R.W.H. (1989). The influence of pre-existing basin structure on thrust system
444 evolution in Western Alps. *Geological Society Special Publications*, 44, 105-122.

445 Butler, R.W.H. (1992). Thrust zone kinematics in a basement-cover imbricate stack; eastern
446 Pelvoux Massif, French Alps. *Journal of Structural Geology*, 14, 29-40.

447 Ceriani, S. (2001). A combined study of structure and metamorphism in the frontal Penninic
448 units between the Arc and the Isère valleys (Western Alps): Implications for the
449 geodynamics evolution of the Western Alps. Unpublished PhD thesis, Universität Basel,
450 196 pp.

451 Ceriani, S., Fügenschuh, B., Potel, S. & Schmid, S.M. (2003). The tectono-metamorphic
452 evolution of the Frontal Penninic units of the Western Alps: correlation between low-
453 grade metamorphism and tectonic phases. *Schweizerische Mineralogische und*
454 *Petrographische Mitteilungen*, 83, 111-131.

455 Ceriani, S., Fügenschuh, B. & Schmid, S.M. (2001). Multi-stage thrusting at the “Penninic
456 Front” in the Western Alps between Mont Blanc and Pelvoux massifs. *International*
457 *Journal of Earth Sciences*, 90, 685-702.

458 Coward, M.P., Gillcrist, R. & Trudgill, B. (1991). Extensional structures and their tectonic
459 inversion in the Western Alps. *Geological Society Special Publications*, 5, 93-112.

460 Dalla Torre, M., Stern, W.B. & Frey, M. (1994). Determination of white K-mica polytype
461 ratios: comparison of different XRD methods. *Clay Minerals*, 29, 717-726.

462 Davies, V.M. 1982: Interaction of thrusts and basement faults in the French external Alps.
463 *Tectonophysics*, 88, 325-331.

464 Debrand-Passard, S., Courbouleix, S. & Lienhardt, M.-J. (1984). Synthèse géologique du
465 Sud-Est de la France. *Mémoire du Bureau de recherches géologiques et minières*, 126pp.

466 Desmons, J., Compagnoni, R. & Cortesogno, L. (1999). Alpine metamorphism of the Western
467 Alps: II. High-P/T and related pre-greenschist metamorphism. In: Frey, M., Desmons, J.
468 & Neubauer, F. (Eds.): The new metamorphic map of the Alps. *Schweizerische*
469 *Mineralogische und Petrographische Mitteilungen*, 79, 111-134.

470 Ernst, W.G. (1963). Significance of phengitic micas from low grade schists. *American*
471 *Mineralogist*, 48, 1357-1373.

472 Essene, E.J. & Peacor, D.R. (1995). Clay mineral thermometry – a critical perspective. *Clays*
473 *Clay Mineral*, 43, 540-553.

474 Ferreiro Mählmann, R. (1994). Zur Bestimmung von Diagenesehöhe und beginnender
475 Metamorphose-Temperaturgeschichte und Tektogenese des Austroalpins und
476 Süppenninikums in Vorarlberg und Mittelbünden. Universität Frankfurt, *Frankfurter*
477 *Geowissenschaftliche Arbeiten, Serie C 14*, 498 pp.

478 Ferreiro Mählmann, R. (1996). The pattern of diagenesis and metamorphism by vitrinite
479 reflectance and illite-“crystallinity” in Mittelbünden and in the Oberhalbstein. Part2:
480 Correlation of coal petrographical and of mineralogical parameters. *Schweizerische*
481 *Mineralogische und Petrographische Mitteilungen*, 76, 23-46.

482 Ferreiro Mählmann, R. (2001). Correlation of very low-grade data to calibrate a thermal
483 maturity model in a nappe tectonic setting, a case study from the Alps. *Tectonophysics*,
484 334, 1-33.

- 485 Ferreiro Mählmann, R. & Frey, M. (2012). “Standardisation, calibration and correlation of the
486 Kübler-Index and the vitrinite/bituminite reflectance measure: a inter-laboratory and field
487 related study”. *Swiss Journal of Geosciences*, this volume.
- 488 Ferreiro Mählmann, R., Bozkaya, O., Potel, S., Le Bayon, R., Šegvić, B. & Nieto García, F.
489 (2012). The pioneer work of Bernard Kübler and Martin Frey in very low-grad
490 metamorphic terranes: Paleo-geothermal potential of Kübler-Index/organic matter
491 reflectance correlation – a review. *Swiss Journal of Geosciences*, this volume.
- 492 Frey, M. (ed.) (1987). *Low Temperature Metamorphism*. Blackie & Son, Glasgow and
493 London, 351 pp.
- 494 Frey, M., de Capitani, C. & Liou, J.G. (1991). A new petrogenetic grid for low-grade
495 metabasites. *Journal of Metamorphic Geology*, 9, 497-509.
- 496 Frey, M., Desmons, J. & Neubauer, F. (Eds.) (1999). The new metamorphic map of the Alps.
497 *Schweizerische Mineralogische und Petrographische Mitteilungen*, 79, 230 pp.
- 498 Frey, M., Teichmüller, M., Teichmüller, R., Mullis, J., Künzi, B., Breitschmid, A., Gruner, U.
499 & Schwizer, B. (1980). Very low-grade metamorphism in external parts of the Central
500 Alps: Illite crystallinity, coal rank and fluid inclusion data. *Eclogae Geologicae*
501 *Helveticae*, 73, 173-203.
- 502 Fügenschuh, B. & Schmid, S. (2003). Late stages of deformation and exhumation of an
503 orogen constrained by fission-track data: A case study in the Western Alps. *Geological*
504 *Society of America Bulletin*, 115, 1425-1440.
- 505 Gillcrist, R., Coward, M. & Mugnier, J.L. (1987). Structural inversion and its controls;
506 examples from the Alpine Foreland and the French Alps. *Geodinamica Acta*, 1, 5-34.
- 507 Guggenheim, S.Jr, Bain, D.C., Bergaya, F., Brigatti, M.F., Drits, V.A., Eberl, D.D., Formoso,
508 M.L.L., Galan, E., Merriman, R.J., Peacor, D.R., Stanjek, H. & Watanabe, T. (2002).
509 Report of the association internationale pour l'étude des argiles (AIPEA) nomenclature

510 committee for 2001: order, disorder and crystallinity in phyllosilicates and the use of the
511 'crystallinity index'. *Clays and Clay Minerals*, 50, 406-409.

512 Guidotti, C.V. & Sassi, F.P. (1986). Classification and correlation of Metamorphic Facies
513 Series by Means of Muscovite b_0 data from Low-Grade Metapelites. *Neues Jarbuch*
514 *Mineralogie Abteilunghefte*, 153, 363-380.

515 Guidotti, C.V., Sassi, F.P. & Blencoe, J.G. (1989). Compositional controls on the a and b cell
516 dimensions of $2M_1$ Muscovites. *European Journal of Mineralogy*, 1, 71-84.

517 Gupta, S. (1997). Tectonic control on paleovalley incision at the distal margin of the early
518 Tertiary Alpine foreland basin, southeastern France. *Journal of Sedimentary Research*,
519 67, 1030-1043.

520 Hall D. L., Sterner S. M. & Bodnar R. J. (1988). Freezing point depression of NaCl-KCl-
521 H₂O solutions. *Economic Geology*, 83, 197-202.

522 Henrichs, C. (1993). Sedimentpetrographische Untersuchungen zur Hochdiagenese in der
523 Kössen-Formation (Ober Trias) der westlichen Ostalpen und angrenzenden
524 Südalpengebiete. *Bochumer geologische und geo-technische Arbeiten* 40, 206 pp.

525 Huyghe, P. & Mugnier, J.L. (1995). A comparison of inverted basins of the southern North
526 Sea and inverted structures of the external Alps. *Geological Society Special Publications*,
527 88, 339-353.

528 Kisch, H.J., Árkai, P. & Brime, C. (2004). On the calibration of illite Kübler index (illite
529 'crystallinity'). *Schweizerische Mineralogische und Petrographische Mitteilungen*, 84,
530 323-331.

531 Kretz, R. (1983). Symbols for rock-forming minerals. *American Mineralogist*, 68, 277-279.

532 Kübler, B. (1964). Les argiles, indicateurs de métamorphisme. *Institut Français Pétrole*, 19,
533 1093-1112.

534 Kübler, B. (1968). Evaluation quantitative du métamorphisme par la cristallinité de l'illite.
535 Etat des progrès réalisés ces dernières années. *Bulletin Centre Recherche Pau, S.N.P.A.*,
536 2, 385-397.

537 Lazarre, J., Tricart, P., Courrioux, G. & Ledru, P. (1996). Héritage téthysien et polyphasage
538 alpin; réinterprétation tectonique du "synclinal" de l'aiguille de Morges (massif du
539 Pelvoux, Alpes occidentales, France). *Comptes Rendus de l'Académie des Sciences, Série*
540 *II. Sciences de la Terre et des Planètes*, 323, 1051-1058.

541 Merriman, R.J., Roberts, B. & Peacor, D.R. (1990). A transmission electron microscope study
542 of white mica crystallite size distribution in a mudstone to slate transitional sequence,
543 North Wales, U. K. *Contributions to Mineralogy & Petrology*, 106, 27-40.

544 Merriman, R.J. & Peacor, D.R. (1999). Very low-grade metapelites: mineralogy, microfabrics
545 and measuring reaction progress. In: Frey, M. & Robinson, D. (Eds.): *Low-Grade*
546 *Metamorphism*. Blackwell Science, London, 10-60.

547 Mullis, J. (1976). Das Wachstumsmilieu der Quarzkristalle im Val d'Illiez (Wallis, Schweiz).
548 *Schweizerische Mineralogische und Petrographische Mitteilungen*, 56, 219-268.

549 Mullis, J. (1987). Fluid inclusion studies during very low-grade metamorphism. In: Frey, M.
550 (Ed.): *Low temperature metamorphism*. Glasgow, Blackie, 162-199.

551 Mullis, J. J., Rahn, M. K. W., Schwer, P., de Capitani, C., Stern, W.B. & Frey, M. (2002).
552 "Correlation of fluid inclusion temperatures with illite "crystallinity" data and clay
553 mineral chemistry in sedimentary rocks from the external part of the Central Alps."
554 *Schweizerische Mineralogische und Petrographische Mitteilungen*, 82, 325-340.

555 Oberhänsli, R., Bousquet, R., Engi, M., Goffé, B., Gosso, G., Handy, M., Höck, V., Koller,
556 F., Lardeaux, J.-M., Polino, R., Rossi, P., Schuster, R., Schwarz, S. & Spalla, M.I.
557 (2004). *Metamorphic structure of the Alps (1:1'000'000)*, Commission for the Geological
558 Map of the World (UNSECO), Paris.

- 559 Perriaux, J. & Uselle, J.P. (1968). Quelques données sur la sédimentologie des grès du
560 Champsaur (Hautes-Alpes). *Géologie Alpine*, 44, 329-332.
- 561 Potel, S., Schmidt, S.Th. & de Capitani, C. (2002). Composition of pumpellyite, epidote and
562 chlorite from New Caledonia – How important are metamorphic grade and whole-rock
563 composition? *Schweizerische Mineralogische und Petrographische Mitteilungen*, 82,
564 229-252.
- 565 Potel S., Ferreiro Mählmann R., Stern W.B., Mullis J. & Frey M. (2006). Very low-grade
566 metamorphic evolution of pelitic rocks under high-pressure/low-temperature conditions,
567 NW New Caledonia (SW Pacific). *Journal of Petrology*, 47, 991-1015.
- 568 Rahn, M.K.W. (2001). The metamorphic and exhumation history of the Helvetic Alps,
569 Switzerland, as revealed by apatite and zircon fission tracks. Unpublished Habilitation
570 thesis, Albert-Ludwigs-Universität Freiburg, 140pp.
- 571 Ravenne, C., Vially, R., Riche, P. & Tremolieres, P. (1987). Sédimentation et tectonique dans
572 le bassin marin Eocene supérieur-Oligocene des Alpes du Sud. *Revue de l'Institut*
573 *Français du Pétrole*, 42, 529-553.
- 574 Sassi, F.P. & Scolari, A. (1974). The b_0 of the potassic white micas as a barometric indicator
575 in low-grade metamorphism of pelitic schists. *Contributions to Mineralogy and*
576 *Petrology*, 45, 143-152.
- 577 Schmid, S.M., Fügenschuh, B., Kissling E. & Schuster, R. (2004). Tectonic map and overall
578 architecture of the Alpine orogen. *Eclogae Geologicae Helvetiae* 97, 93-117.
- 579 Seward, D., Ford, M., Bürgisser, J., Lickorish, H., Williams, E.A. & Meckel III L.D. (1999).
580 Preliminary report on fission tracks studies in the Pelvoux area, SE France. *Memorie di*
581 *Scienze Geologiche*, 51, 25-31.
- 582 Sue, C., Tricart, P., Dumont, T. & Pecher, A. (1997). Raccourcissement polyphase dans le
583 massif du Pelvoux (Alpes occidentales) : exemple du chevauchement de socle de Villard-

584 Notre-Dame. *Comptes Rendus de l'Académie des Sciences, Série II. Sciences de la Terre*
585 *et des Planètes*, 324, 847-854.

586 Tagami, T., Galbraith, R. F., Yamada, R. & Laslett, G. M. (1998). Revised annealing kinetics
587 of fission tracks in zircon and geological implications. In P. Van den haute, & F. De
588 Corte (Eds.), *Advances in fission-track geochronology*: Kluwer academic publishers,
589 Dordrecht, The Netherlands, 99-112.

590 Tricart, P. (1986). Le Chevauchement de la zone briançonnaise au Sud-Est du Pelvoux; clé
591 des rapports zone externe - zones internes dans les Alpes occidentales. *Bulletin de la*
592 *Société Géologique de France, Huitième Série*, 2, 233-244.

593 Tricart, P., Bourbon, M., Chenet, P. Y., Cros, P., Delorme, M., Dumont, T., Graciansky, P.C.,
594 Lemoine, M., Megard, Galli, J. & Richez, M. (1988). Tectonique synsédimentaire
595 triasico-jurassique et rifting téthysien dans la nappe briançonnaise de Peyre-Haute (Alpes
596 occidentales). *Bulletin de la Société Géologique de France*, 4, 669-680.

597 Tricart, P., Bouillin, J.P., Dick, P., Moutier, L. & Xing, C. (1996). Le faisceau de failles de
598 haute-Durance et le rejeu distensif du front briançonnais au SE du Pelvoux (Alpes
599 occidentales). *Comptes Rendus de l'Académie des Sciences, Série II. Sciences de la Terre*
600 *et des Planètes*, 323, 251-257.

601 Tricart, P. (2004). From extension to transpression during the final exhumation of the Pelvoux
602 and Argentera massifs, Western Alps. *Eclogae Geologicae Helvetiae*, 97, 429-439.

603 Tricart, P., Schwartz, S., Sue, C., Poupeau, G. and Lardeaux, J.M. (2001). La dénudation
604 tectonique de la zone Ultradaphinoise et l'inversion du front Briançonnais au Sud Est du
605 Pelvoux (Alpes Occidentales); une dynamique Miocène à actuelle. *Bulletin de la Société*
606 *Géologique de France*, 172, 49-58.

607 Trullenque, G. (2005). Tectonic and microfabric studies along the Penninic Front between
608 Pelvoux and Argentera Massifs (Western Alps, France). Unpublished PhD thesis,
609 Universität Basel, 301 pp.

610 Trullenque, G., Kunze, K., Heilbronner, R., Stünitz, H. & Schmid, S. (2006). Microfabrics of
611 calcite ultramylonites as records of coaxial and non-coaxial deformation kinematics:
612 Examples from the Rocher de l'Yret shear zone (Western Alps). *Tectonophysics*, 424, 69-
613 97.

614 Waibel, A.F. (1990). Sedimentology, petrographic variability, and very-low-grade
615 metamorphism of the Champsaur sandstone (Paleogene, Hautes-Alpes, France).
616 Evolution of volcanoclastic foreland turbidites in the external Western Alps. Unpublished
617 PhD thesis, Université de Genève, 140pp.

618 Warr, L.N. & Rice, A.H. (1994). Interlaboratory standardization and calibration of clay
619 mineral crystallinity and crystallite size data. *Journal of Metamorphic Geology*, 12, 141-
620 152.

621 Yamada, R., Tagami, T., Nishimura, S. & Ito, H. (1995). Annealing kinetics of fission tracks
622 in zircon: an experimental study. *Chemical Geology (Isotope Geoscience Section)*, 122,
623 249-258.

624 Yamada, R., Galbraith, R.F., Murakami, M., Tagami, T. (2007). Statistical modelling of
625 annealing kinetics of fission-tracks in zircon; reassessment of laboratory experiments.
626 *Chemical Geology*, 236, 75-91.

627 Zhang, Y. & Frantz, J. D. (1987). Determination of the homogenization temperatures and
628 densities of supercritical fluids in the system NaCl-KCl-CaCl₂-H₂O using synthetic fluid
629 inclusions. *Chemical Geology*, 64, 335-350.

630

631 **Fig. 1:** (a) Simplified geological overview of the arc of the western Alps (A: Argentera
632 massif, CM: Combeynot massif, MB: Mont Blanc massif, P: Pelvoux massif, R: Rhone-
633 Simplon line, T: Tonale line); after Froitzheim et al. (1996), Ceriani et al. (2000) and Schmidt
634 et al. (2004). (b) Tectonic map along the eastern rim of the Pelvoux Massif compiled from 1)
635 geological maps BRGM (1/50 000): La Grave, Briançon, St Christophe en Oisans, Guillestre,
636 Orcières and Embrun and 2) Tricart (1986). Points Yr, Fo, Be, Cha, Do and DoF refer to
637 samples studied, collected at the eastern rim of the Pelvoux Massif, in the Yret, Fournel,
638 Beassac, Chambran, Dormillouse and Dormillouse-Fangeas valleys, respectively. RT:
639 Roselend Thrust. RYSZ: Rocher de l'Yret shear zone.

640

641 **Fig. 2:** Distribution and values of Kübler index (KI) and Árkai index (ÁI) in the studied area.
642 Due to the proximity of the samples Do4,4a,4b; Do5a,c; DoF1a,b; Fo1b,c,e; Fo2b,c and
643 Fo3a,b,c the values are shown as averages. RT: Roselend Thrust.

644

645 **Fig. 3:** Correlation between Kübler index (KI) and Árkai index (ÁI) (a) and the $2M_1/1M_d$
646 illite polytype ratio (b), all derived from air-dried mounts.

647

648 **Fig. 4:** Cumulative curves of K-white mica *b* cell dimensions for 21 anchizonal samples from
649 our study area (in bold) with reference curves from Sassi and Scolari (1974) and Guidotti and
650 Sassi (1986).

651

652 **Fig. 5:** Depth-Temperature diagrams with isochores representing the higher and the lower
653 calculated molar volumes for vapour-rich fluid inclusions and the mean isochores in samples
654 F72 (a) and F92 (b) from the Yret zone. The dashed lines represent the range of geothermal

655 gradients from 25°C/km and 35°C/km as deduced from the K-white mica *b* cell dimensions.

656 The thick curve represents the liquid-gas reaction curve of water. CP: critical point of water.

657

658 **Table 1:** Samples identification, stratigraphic age, Illite Kübler index and chlorite

659 "crystallinity" values of the <2µm grain-size fraction samples (data in $\Delta^{\circ}2\theta$), percent of 2M₁

660 polytypes and K-white mica *b* cell dimension data.

661

662 **Table 2:** Fluid inclusion data of two quartz samples from the Yret Zone, Western French

663 Alps.

664

665

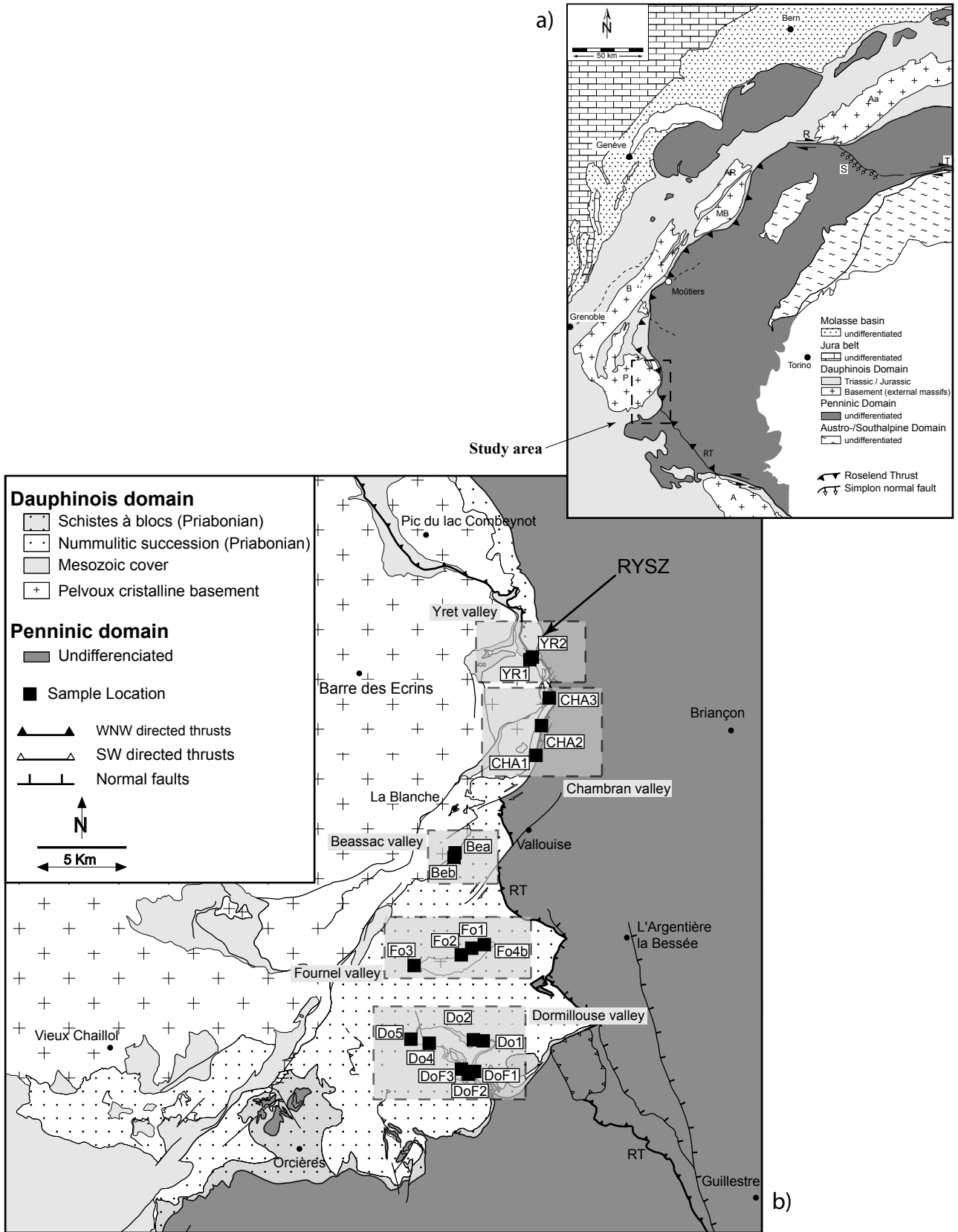


Figure 1

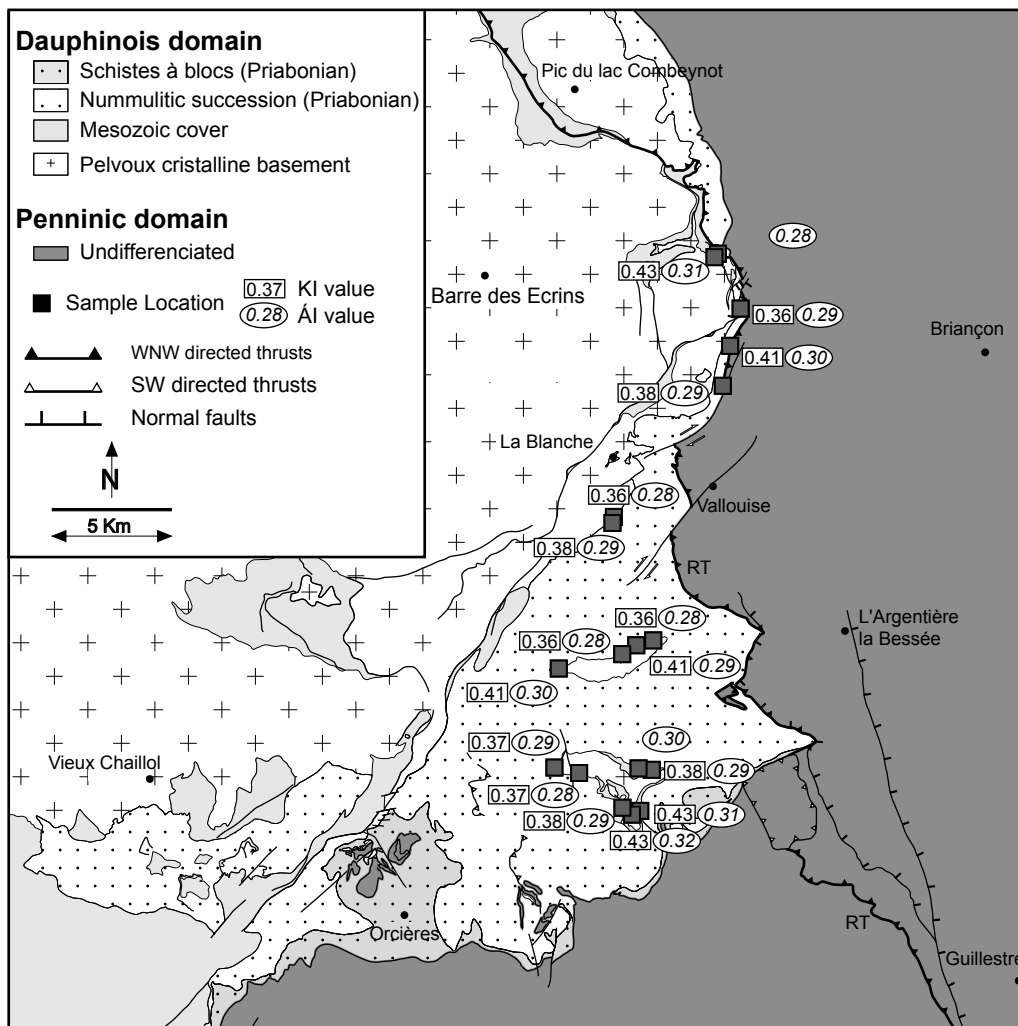


Figure 2

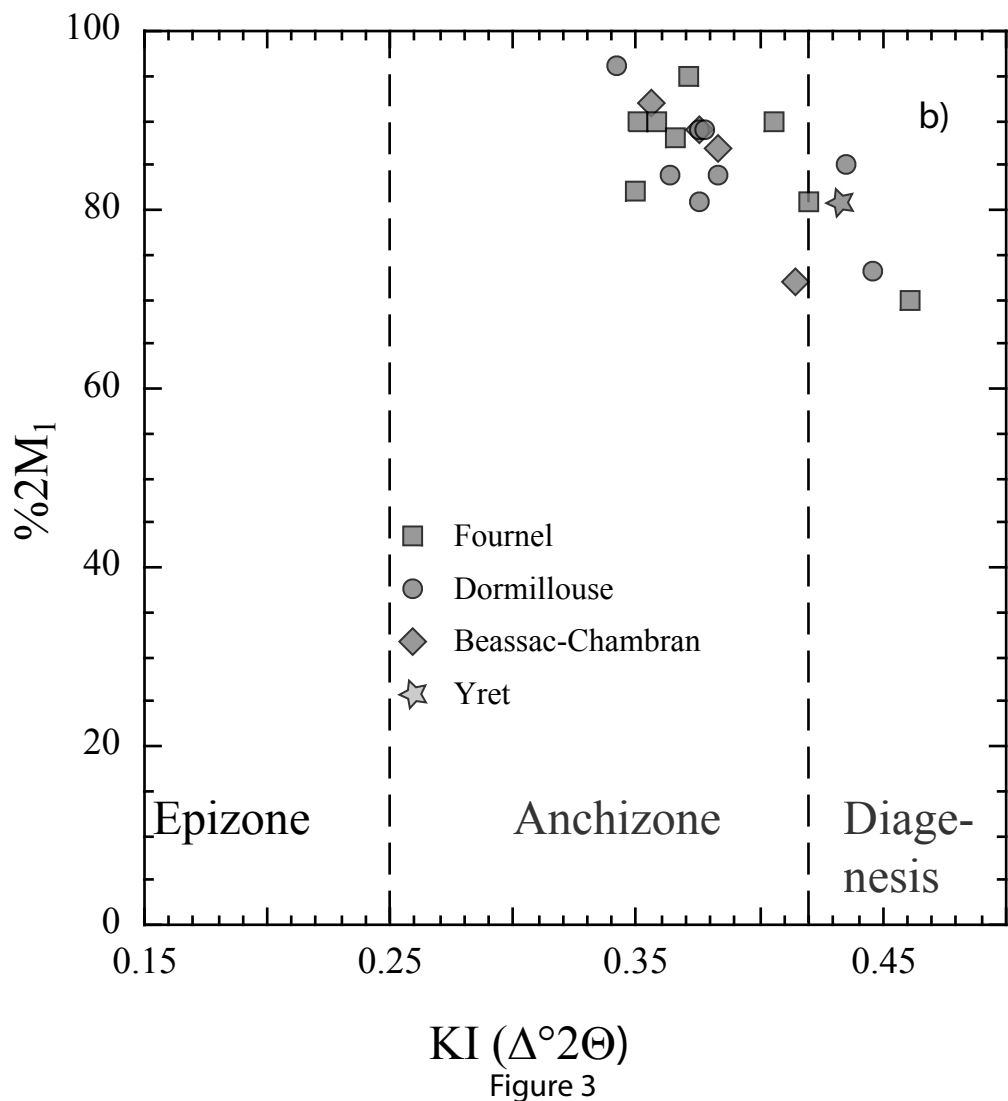
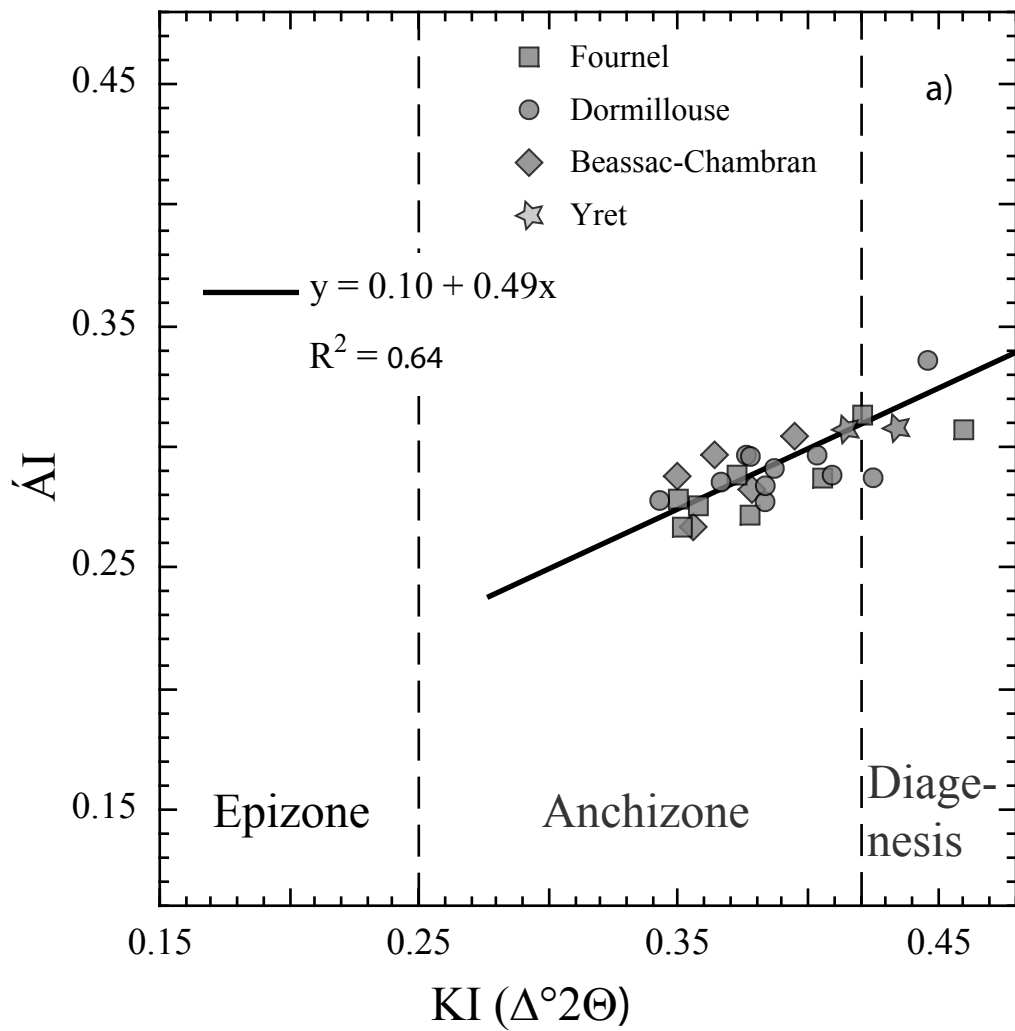


Figure 3

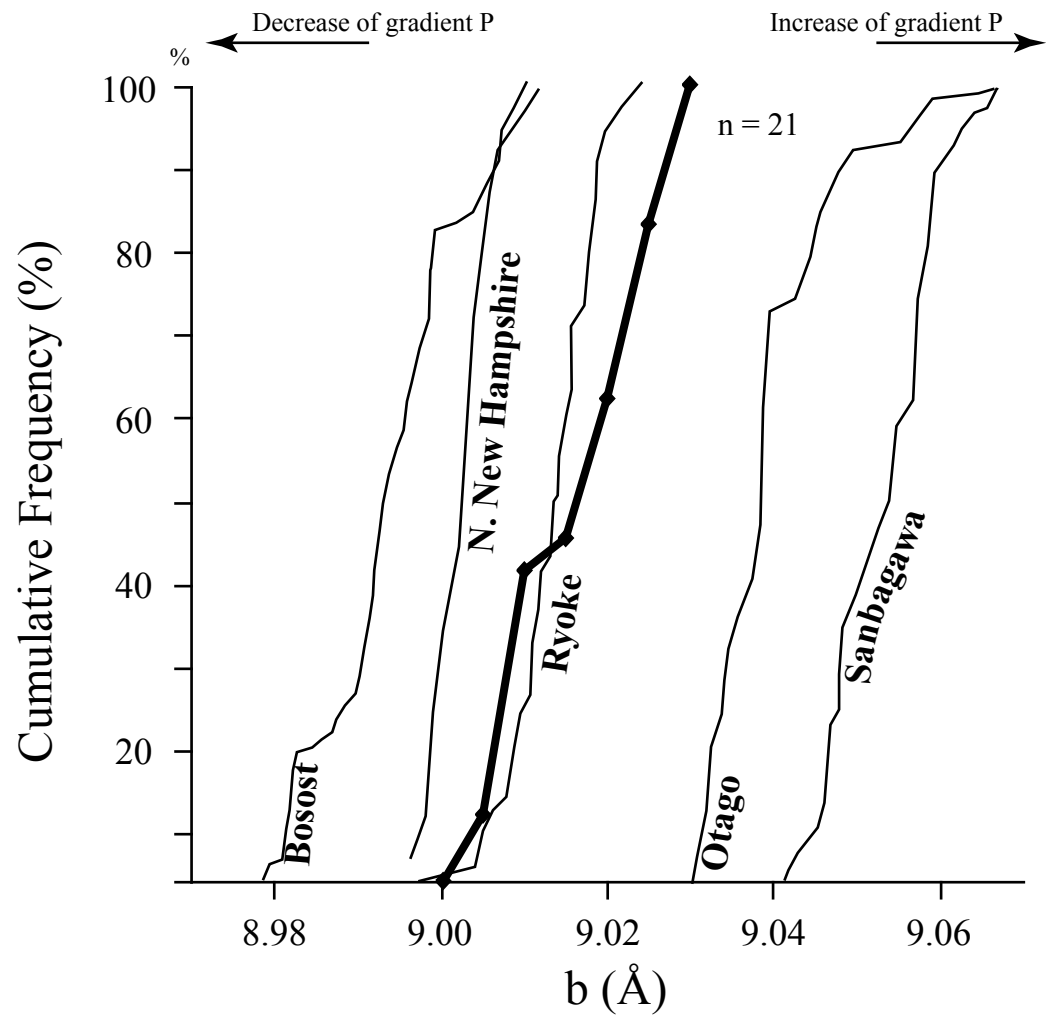


Figure 4

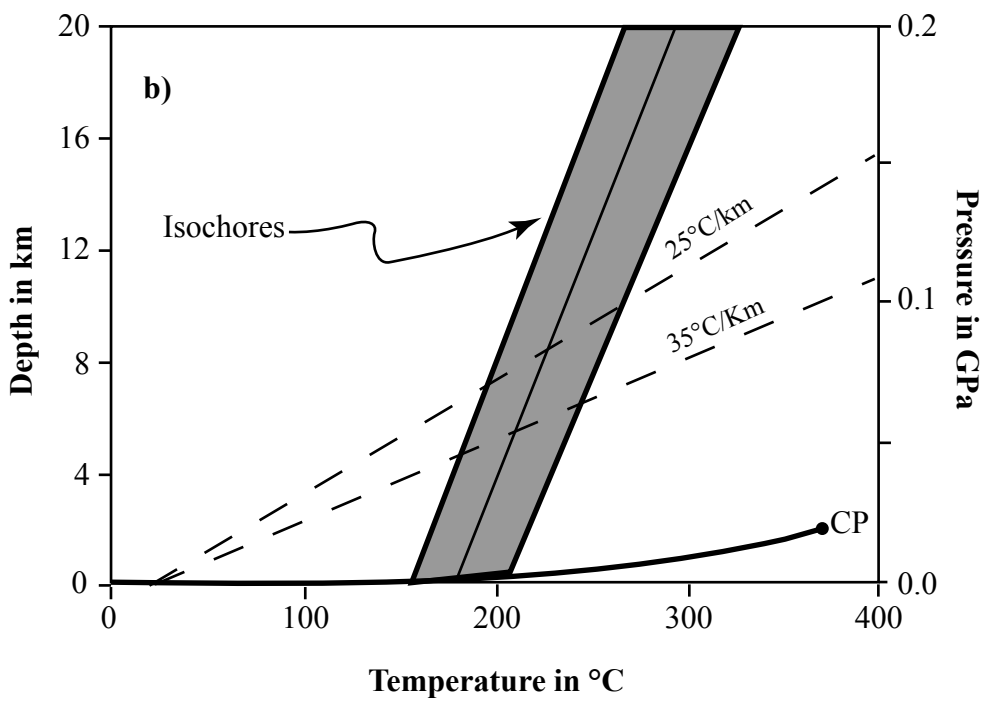
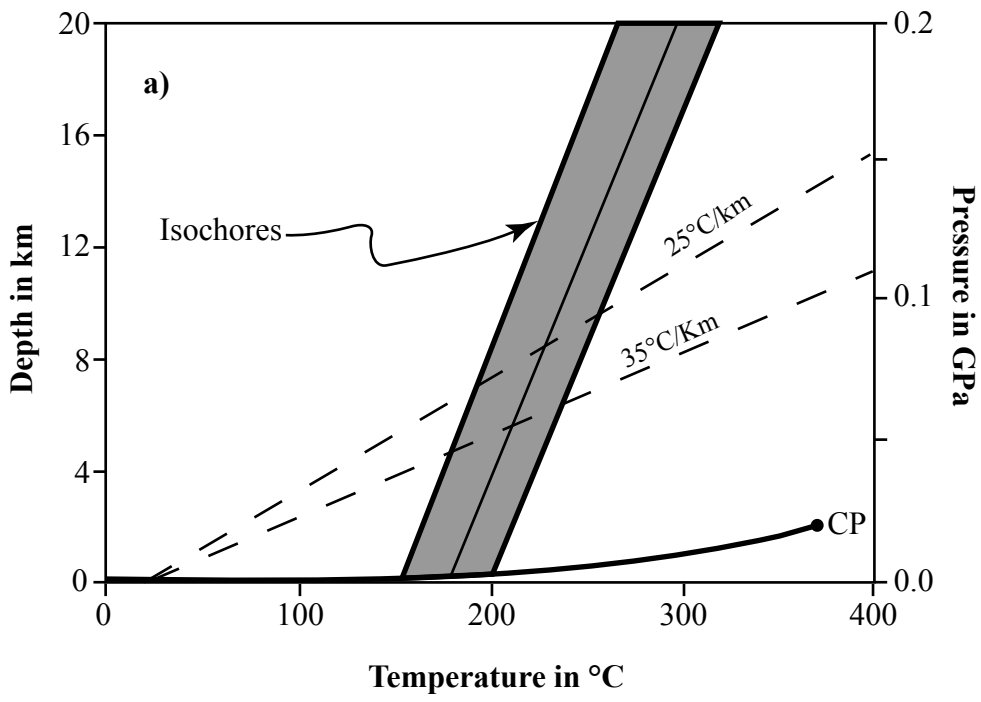


Figure 5

Sample	Sratigraphic age	Elevation in m	IC _{Giessen} Δ°2Θ	KI Δ°2Θ	1σ Δ°2Θ	ChC Δ°2Θ	ÁI Δ°2Θ	1σ Δ°2Θ	%2M ₁	b (Å)
Bea	Priabonian	1350	0.31	0.36	0.00	0.30	0.28	0.00	92	9.024
Beb	Priabonian	1370	0.33	0.38	0.00	0.30	0.29	0.01	87	9.009
CHA1	Priabonian	1700	0.33	0.38	0.01	0.30	0.29	0.01	89	9.008
CHA2	Priabonian	1710	0.36	0.41	0.00	0.32	0.30	0.01	72	9.015
CHA3	Priabonian	1720	0.32	0.36	0.00	0.30	0.29	0.01	84	9.001
Do1	Mesozoic Cover	1500	0.33	0.38	0.00	0.30	0.29	0.00	81	8.998
Do2	Mesozoic Cover	1520	0.35	0.40	0.00	0.32	0.30	0.01	-	9.006
Do4a	Priabonian	1835	0.33	0.38	0.00	0.30	0.29	0.01	-	9.026
Do4b	Priabonian	1835	0.34	0.39	0.01	0.30	0.29	0.01	-	9.025
Do4	Priabonian	1840	0.30	0.34	0.01	0.29	0.28	0.01	96	9.010
D05a	Mesozoic Cover	2100	0.33	0.38	0.00	0.31	0.30	0.01	89	9.004
Do5c	Mesozoic Cover	2105	0.32	0.37	0.01	0.31	0.29	0.01	79	9.007
DoF1a	Mesozoic Cover	1700	0.35	0.41	0.00	0.32	0.30	0.01	-	-
DoF1b	Mesozoic Cover	1700	0.38	0.45	0.00	0.33	0.32	0.02	73	-
DoF2	Priabonian	2400	0.37	0.43	0.00	0.34	0.32	0.02	85	-
DoF3	Priabonian	2200	0.33	0.38	0.00	0.30	0.29	0.00	84	9.025
Fo1b	Priabonian	1800	0.32	0.37	0.00	0.30	0.28	0.01	88	9.018
Fo1c	Priabonian	1740	0.31	0.35	0.00	0.29	0.28	0.02	90	9.010
Fo1e	Priabonian	1740	0.33	0.38	0.00	0.30	0.28	0.01	-	-
Fo2b	Priabonian	1760	0.32	0.37	0.00	0.30	0.28	0.01	95	9.017
Fo2c	Priabonian	1760	0.31	0.36	0.00	0.30	0.29	0.01	90	9.019
Fo3a	Priabonian	2100	0.31	0.35	0.00	0.29	0.28	0.01	82	9.028
Fo3b	Priabonian	2100	0.36	0.42	0.00	0.32	0.31	0.01	81	9.025
Fo3c	Priabonian	2100	0.39	0.46	0.02	0.32	0.31	0.01	70	-
Fo4b	Priabonian	1640	0.35	0.41	0.00	0.31	0.29	0.01	90	9.016
YR1	Priabonian	2700	0.37	0.43	0.01	0.33	0.31	0.00	81	9.021
YR2	Priabonian	2700	0.34	0.39	0.01	0.29	0.28	0.01	-	-

IC= illite “crystallinity” measured in Giessen. KI= Kübler Index. ChC= chlorite “crystallinity” of the 002 chlorite peak. ÁI= Árkai Index. %2M₁= percent of 2M₁ polytypes. b(Å)= K-white mica *b* cell dimension.

Table 2

1	2	3	4	5	6	7	8	9	10
Locality	FP	HM	IT	n_l	V%	Tm_{ICE}	Th_l	H₂O mole %	NaCl mole %
F72	1	FQ	P	66	5	-3.5 ± 0.6	176.6 ± 18.3	94.5	5.6
F92	1	VQ	Ps II	22	5	-6.9 ± 0.9	182.4 ± 15.5	89.8	10.2
“	2	VQ	P	3	5-10	-9.6 ± 0.9	172.3 ± 10.0	87.2	13.8

(1) Locality number. (2) FP = Fluid inclusion population. (3) HM = Host mineral. - FQ = Fibre quartz; VQ = Vein quartz. (4) IT = Inclusion type. - Ps II = Pseudosecondary fluid inclusions; P = Primary fluid inclusions. (5) n_l = Number of measured fluid inclusions. (6) V % = Volume-% of the volatile part estimated at room temperature. (7) Tm_{ice} = Melting temperature of ice (°C). - *First number* = mean value; *second number* = standard deviation. (8) Th_l = Homogenization temperature of fluid inclusions. - First number = mean value; second number = standard deviation. (9) and (10) = Approximate mole-% H₂O and NaCl (equivalents).